Supporting Information

Mortimer et al. 10.1073/pnas.0900715106

SI Text

Bayesian Gradient Sensing Model. We consider the model 1-dimensional gradient sensing device shown in Fig. S1. The positions of the bound receptors are given by the multiset $\mathcal{B}$, and the multiset $\mathcal{R}$ denotes the positions of all receptors regardless of binding state. The external gradient is described by the parameters γ and μ, where γ is the concentration at the center of the receptor array given in dimensionless units, $\gamma = C/K_d$, where K_d is the dissociation constant of the receptors. The parameter μ is the relative change in concentration across the spatial extent of the array. We assume that each receptor's binding state is independent of those around it, so that the likelihood function $P(\mathcal{B},U|\gamma, \mu, \mathcal{R})$ is the product of likelihood functions for each receptor individually, conditioned on the fact that $\mathcal{R}$ must contain $\mathcal{B}$:

$$P(\mathcal{B}|\gamma, \mu, \mathcal{R}) = \chi(\mathcal{B} \subset \mathcal{R}) \prod_{r\in\mathcal{B}} \frac{\gamma(1+\mu r)}{1+\gamma(1+\mu r)} \prod_{r\in\mathcal{R}/\mathcal{B}} \frac{1}{1+\gamma(1+\mu r)} = \chi(\mathcal{B} \subset \mathcal{R}) \frac{\gamma^n}{(1+\gamma)^N} \prod_{r\in\mathcal{B}} \frac{1+\mu r}{1+\mu pr} \prod_{r\in\mathcal{R}/\mathcal{B}} \frac{1}{1+\mu pr},$$

where $n = |\mathcal{B}|$ is the number of bound receptors, $N = |\mathcal{R}|$ is the total number of receptors, $\chi(\mathcal{B} \subset \mathcal{R})$ is one when $\mathcal{B}$ is a subset of $\mathcal{R}$, and zero otherwise, $\rho = \gamma/(1+\gamma)$ is the probability that a receptor at $r = 0$ is bound, and $\mathcal{R}/\mathcal{B} = \{x \in \mathcal{R} | x \notin \mathcal{B}\}$.

We can then calculate the posterior distribution for μ:

$$P(\mu|\mathcal{B}) \propto P(\mu) \int_0^\infty d\gamma P(\gamma) \frac{\gamma^n}{(1+\gamma)^N} \int d^N\mathcal{R} P(\mathcal{R}) \chi(\mathcal{B} \subset \mathcal{R}) \prod_{r\in\mathcal{B}} \frac{1+\mu r}{1+\mu pr} \prod_{r\in\mathcal{R}/\mathcal{B}} \frac{1}{1+\mu pr}.$$

Assuming that $P(\mu)$ is symmetric and is concentrated around zero (i.e., we are interested in guidance under shallow gradient conditions) and that receptors are distributed independently of one another [i.e., $P(\mathcal{R}) = \Pi_{r\in\mathcal{R}} P(r)$], we can make a Taylor approximation to first order in μ, obtaining:

$$P(\mu|\mathcal{B}) \propto P(\mu) \int_0^\infty d\gamma P(\gamma) \frac{\gamma^n}{(1+\gamma)^N} \int d^N\mathcal{R} P(\mathcal{R}) \chi(\mathcal{B} \subset \mathcal{R}) \exp(\mu(R_b - \rho R))$$

$$= P(\mu) \int_0^\infty d\gamma P(\gamma) \frac{\gamma^n}{(1+\gamma)^N} \exp((1-\rho)\mu R_b) \int d^{N-n}U P(U) \exp(-\mu\rho R_u)$$

where $R_b = \Sigma_{r\in\mathcal{B}} r$, $R_u = \Sigma_{r\in\mathcal{R}/\mathcal{B}} r$, and $R = \Sigma_{r\in\mathcal{R}} r$.

Finally, assuming that there are a sufficient number of receptors to obtain a good estimate of the ambient concentration, we obtain:

$$P(\mu|\mathcal{B}) \propto P(\mu) \exp[(1-\hat{\rho})\mu R_b]$$

where $\hat{\rho}$ is the a posteriori mean estimate for ρ, assuming that no gradient is present:

$$\hat{\rho} = \int_0^\infty d\gamma P(\gamma) \frac{\gamma^n}{(1+\gamma)^N} \rho.$$

Thus, by inspection, we find that the sensing device's optimal estimate of the sign of μ is given by $\text{sign}[(1-\hat{\rho})R_b] = \text{sign} R_b$.

For given gradient conditions, (γ, μ), many different patterns of binding $\mathcal{B}$ may be observed, with probability $P(\mathcal{B}|\gamma, \mu)$. By applying the optimal strategy derived above, the gradient sensor maximizes its chances of correctly estimating the gradient direction. However, because receptor binding is stochastic, there will still be a finite chance that an incorrect conclusion about the gradient direction will be made. A useful measure of the performance of the optimal gradient sensing strategy is thus to estimate the probability with which the correct decision is made under given gradient conditions, $P_{\text{correct}}(\gamma, \mu) = P(R_b > 0|\gamma, \mu)$.

Because R_b is obtained by summing many independent variables with finite variance and mean together, by the central limit theorem, we can approximate $P(R_b|\gamma, \mu)$ with a Gaussian distribution centered on $\langle R_b \rangle$ and with variance $\text{var}(R_b)$.

Assuming that receptors are distributed uniformly along the sensor, then for shallow gradients, we can approximate the mean of R_b to first order in μ with:

$$\langle R_b \rangle = \sum_i \langle r_i b_i \rangle$$

$$= N \int_{-1/2}^{1/2} dr P(r) P(b = 1|r, \gamma, \mu) r$$

$$\approx N\rho(1-\rho)\langle r^2 \rangle \mu.$$

We only need the zeroth order terms for the variance of R_b. We have:

$$\begin{aligned}\mathrm{var}(R_b) &= \mathrm{var}\left(\sum_i r_i b_i\right)\\ &= \sum_{i,j}\left(\langle r_i r_j b_i b_j\rangle - \langle r_i b_i\rangle\langle r_j b_j\rangle\right)\\ &= \sum_{i=j}\left(\langle r_i^2 b_i^2\rangle - \langle r_i b_i\rangle^2\right)\end{aligned}$$

where, because $b = 0$ or 1, we know that $b^2 = b$. Thus we have:

$$\begin{aligned}\mathrm{var}(R_b) &= N(\langle r^2 b\rangle - \langle rb\rangle^2)\\ &= N\left[\left(\int_{-1/2}^{1/2} drP(r)P(b=1|r,\ \gamma,\ \mu)r^2\right) - \left(\int_{-1/2}^{1/2} drP(r)P(b=1|r,\ \gamma,\ \mu)r\right)^2\right]\\ &\approx N\rho\langle r^2\rangle,\end{aligned}$$

where $\langle r^2\rangle = \int drP(r)r^2 = 1/12$.

By using this Gaussian approximation for $P(R_b|\gamma,\ \mu)$, the performance can be approximated by:

$$\begin{aligned}P_{correct}(\gamma,\ \mu) &= \int_0^\infty dR_b P(R_b|\gamma,\ \mu)\\ &\approx \frac{1}{2}\,\mathrm{erfc}\left(-\frac{\langle R_b\rangle}{\sqrt{2\mathrm{var}(R_b)}}\right)\\ &\approx \frac{1}{2} + \mu\sqrt{\frac{N}{24\pi}}\,\sqrt{\rho}\,(1-\rho),\end{aligned}$$

and $\langle R_b\rangle/\sqrt{2\langle R_b^2\rangle} = \mu\sqrt{N/24\pi}\sqrt{\rho}(1-\rho)$ is identified as the signal-to-noise ratio for gradient detection. Replacing ρ in this expression with $\gamma/(1+\gamma)$ gives the formula used in the main text.

Concentration and Steepness Correction for Printed Gradients. We have previously demonstrated (2, 3) that the spatiotemporal distribution of NGF in our printing assay is predictable from the laws of diffusion. The concentration at the explants in the assay is not exactly constant, but varies in a predictable manner with time, by an amount that depends on the gradient steepness. For the gradient steepness (0.2%) principally used in ref. 2, the size of this variation is insignificant compared to the quantization of concentration used in that study ($\log_{10}$ units). However, in the present work, steeper gradients were used, and concentration was quantized more finely (half $\log_{10}$ units), and it thus becomes important to correct for these concentration variations.

The exponential factors we used to determine our stock concentrations of NGF for printing for the experiments reported here were equivalent to 0.1%, 0.2%, 0.3%, and 0.4% per 10 μm. To determine the actual concentrations and steepnesses at the explants, we simulated 12 line gradients as used in the experiment in MATLAB, with initial steepnesses of 0.1%, 0.2%, 0.3% and 0.4% over 48 h, and probed the concentration and steepness at line 4, where the explants are placed in the assay. We assumed that the experimental situation is 2-dimensional, and effectively infinite, and summed a set of point sources representing the individual spots printed onto the collagen. The subsequent variation in concentration and gradient steepness at the explants is shown in Fig. S2 *A* and *B*. It can be seen that concentration increases over time in each case, but more rapidly for higher initial gradient steepness, and that there is an initial rise in gradient steepness, followed by a decay that is more rapid for higher initial steepnesses.

To correct for these effects, we calculated the time-averaged concentration and steepness at the explant as follows:

$$\langle X\rangle = \frac{1}{T}\int_0^t dtX(t) \approx \frac{1}{T}\sum_i X_i\delta t.$$

The resulting correction factors are shown in Fig. S2 *C* and *D*. The average concentration at the explant increases with initial gradient steepness. The average gradient steepness also increases with initial gradient steepness, although the dependence appears to be linear, at least for the small gradient steepnesses used here. These correction factors were applied to the experimental data before they were plotted in Fig. 1*B* in the main paper, because this provides the most accurate estimate of the actual gradient conditions at the explants in the experiment.

Total Outgrowth Depends on Concentration, but This Dependence Does Not Explain the Observed Explant Asymmetry. Despite the fit between model and data evidenced by Fig. 3 of the main text, it is conceivable that the explant asymmetry we observed in our gradients could be simply due to differential responses to absolute levels of NGF between the 2 sides of the explant, rather than being directly mediated by the gradient itself. This could be due to a dependence on NGF concentration of factors such as the total neurite outgrowth, the degree of fasciculation, the degree of branching, and the strength of our antibody staining via changes in microtubule

structure or concentration. It was therefore important for us to eliminate the possibility that such factors could be determining the degree of explant asymmetry observed experimentally, rather than a true directional response to the gradient.

Besides explant asymmetry, we therefore also measured how the total neurite outgrowth from each explant depended on gradient conditions. To quantify total outgrowth, a steerable ridge filter was applied to the nonexplant region of each image and used to generate an independent estimate of the neurite distribution (with pixels located on neurite-like ridges chosen over pixels belonging to more uniform-intensity neighborhoods). A measure of neurite outgrowth was obtained by dividing the total number of pixels corresponding to neurites by the total number of pixels within the explant region. In agreement with Conti et al. (1) and Rosoff et al. (2), we found that outgrowth was biphasic in concentration. In common with the guidance ratio measurements, we found that total neurite outgrowth peaked at ≈0.3 nM NGF for all gradient steepnesses (Fig. S3*A*). In contrast with guidance ratio measurements, we found no difference in peak height for different steepnesses.

However, despite the superficial similarity between the curves in Fig. S3*A*, and those in Fig. 2*B* of the main text, these results actually allow us to eliminate the "trophic" hypothesis using 3 simple quantitative arguments:

1) the trophic effect would sometimes predict asymmetry in the opposite direction to that observed;
2) it would predict a peak of asymmetry at a different NGF concentration from that actually measured; and
3) the trophic effect is in any case too small.

Furthermore, because the guidance ratio is based on pixel counts, and because Fig. S3*A* is also based on pixel counts, these arguments automatically includes all factors that potentially influence pixel counts, including total outgrowth, fasciculation, branching, and microtubule distribution.

In more detail, it can immediately be seen from Fig. S3*A* that the trophic hypothesis incorrectly predicts that explant asymmetry (as measured by the guidance ratio) should be directed down the gradient for concentrations in the range ≈ 0.3–3 nM, because here, pixel counts are decreasing as NGF concentration increases. Second, the trophic hypothesis predicts that the largest explant asymmetry should be seen at NGF concentrations for which the rate of change of outgrowth is largest, i.e., at ≈0.1 nM (positive) and 1 nM (negative). However the measured peak of asymmetry occurs at 0.3 nM, where the outgrowth curve also peaks, and outgrowth is thus changing relatively slowly with NGF concentration.

Thirdly, consider that the largest increase in concentration across an average explant size of 625 μm in our experiments was ≈20% (0.3% gradient). (Although neurites growing from top and bottom of the explant are more widely separated than this by 2 days in culture, this extreme separation does not represent the average conditions under which they were growing.) Fig. S3*A* shows that, even for concentrations at which overall outgrowth changes fastest, a concentration increase of 20% produces only a very small change in outgrowth (data points in Fig. S3*A* are separated by half a log unit, i.e., ≈300%). To estimate the size of this effect more precisely, we considered an explant of diameter D exposed to an NGF gradient such that the concentration at its center is C, and the difference in absolute concentration across the diameter of the explant is ΔC. An estimate of the trophic effect on the guidance ratio can be obtained by approximating the neurite outgrowth on the high- and low-concentration sides of the explant with half the total outgrowth observed from explants subjected to mean concentrations of $C \pm \frac{1}{2}\Delta C$. Assuming that the exponential gradient is close to linear on the scale of the explants, then $\Delta C \approx \frac{D}{d} sC$, where s is the fractional gradient steepness over distance d. By interpolating the curves in Fig. S3*A*, the outgrowth-mediated guidance displayed in Fig. S3*B* was obtained (choosing s/d = 0.003/10 μm and D = 625 μm). Note that the guidance ratio values range between +0.03 and −0.03, which, as predicted, is much smaller than the significant features in the measured guidance response. Recalculating these numbers assuming a wider average separation of neurites growing up and neurites growing down would obviously increase the size of the effect, but would also proportionally magnify the size of the incorrect prediction that the asymmetry should be directed down the gradient for concentrations in the range ≈0.3–3 nM.

Note that the arguments above also discount other explanations for the observed explant asymmetry besides differential outgrowth, such as variations with NGF concentration of branching, fasciculation, and microtubule distribution, because these effects would also be apparent in total pixel counts. The arguments above show that the effect of all purely concentration-dependent influences on pixel counts are small compared with the size of the guidance ratios we measured (and indeed, as already mentioned, predict guidance in the wrong direction for certain NGF concentrations). Thus, we conclude that the explant asymmetry we measured experimentally is primarily due to guidance by the gradient, rather than a dependence of axonal parameters purely on absolute NGF concentration.

Explant Asymmetry Is Primarily Due to Guidance of Neurites, Not Bias in the Direction of Neurite Initiation. To generate our main dataset, we printed the gradient immediately after explants were embedded in the collagen. This leaves open the possibility that the asymmetry in final outgrowth we observed could be due to an effect of the gradient on the direction of neurite initiation rather than guidance of neurites as they extend away from the cell body. To test this possibility, we delayed the application of a 0.3 nM/0.24% NGF gradient for 2–24 h after the explants were embedded with uniform 0.1 nM NGF in the collagen to promote survival. Printed gradients were adjusted to discount this background. Fig. S4*A* shows typical explants at some of these time points before the gradient was added. All explants were then fixed 48 h after embedding. Fig. S4*B* shows that a similar degree of final asymmetry persists even when the gradient is applied up to 18 h after embedding (n and P values in Table S3). This is consistent with the idea that observed explant asymmetries arise from the influence of the gradient on growing neurites, rather than on their initial direction of growth.

This conclusion relies on the assumption that most neurite initiation occurs soon after plating. Evidence for this is provided by the following argument. If all neurite initiation occurred at t = 0 (the time of plating), and then neurites grew at a constant rate, one would expect the total length of neurites to grow linearly with time. Because for dense outgrowth, the total outgrowth scales as roughly the square of neurite length, one would then expect the square root of total outgrowth to vary roughly linearly with time. Fig. S4*C* shows that these are indeed strongly linearly correlated. Thus, we conclude that for most neurons, neurite growth begins at an early time point and, hence, that explant asymmetry predominantly results from the influence of the gradient on already-growing neurites.

Performance of the Optimal Strategy Compared with Other Gradient-Sensing Strategies. For optimal gradient sensing, we have shown that the receptors should be weighted in proportion to their distance from the center of the sensing device. However, in principle, there

are many other ways in which a gradient might be detected. In this section, we first show that all strategies involving the comparison of weighted receptor signals perform worse than our optimal strategy. We then compare the performance to some other possible strategies.

We first consider approximations to the Bayesian model, where receptors produce signals that are weighted according to a function $w(r)$ that depends on the position of the receptor relative to the center of the sensing device. We will assume that $w(r)$ is antisymmetric about $r = 0$, because if it is not, the gradient sensor will be biased for one direction over the other. The direction of the gradient is then estimated based on $R_w = \Sigma_{r\in\mathcal{B}} w(r)$. So, for example, for the optimal strategy, we have $w(r) = r$, whereas a strategy that simply compares the number of bound receptors on each side of the device would have a weighting function $w(r) = \text{sign}(r)$. Calculating performance in the same way as we did for the optimal strategy, we have:

$$\langle R_w \rangle = \sum_i \langle w(r_i) b_i \rangle$$

$$\approx N\rho(1-\rho)\langle w(r) r \rangle \mu$$

and

$$\text{var}(R_w) \approx N\rho\langle w(r)^2 \rangle$$

and thus, the probability of making a correct decision is approximately

$$P_{correct} \approx \frac{1}{2} + \sqrt{\frac{N}{2\pi}} \frac{\langle w(r) r \rangle}{\sqrt{\langle w(r)^2 \rangle}} \sqrt{\rho}(1-\rho).$$

Thus, regardless of the choice of $w(r)$, we obtain a curve whose variation with gradient parameters is given by $\mu\sqrt{\rho}(1-\rho)$, which is the same as that for the optimal strategy. It can also be shown that selecting $w(r) \propto r$ gives the maximum possible performance, verifying our claim that R_b gives the optimal gradient detection strategy. Fig. S6 compares the performance of the optimal strategy to the strategy that compares the number of bound receptors on each side of the sensor.Fig. S6 also shows the (simulated) performance of a different strategy, based on a model we previously suggested in ref. 5 (the red dashed line). Here, signals generated by bound receptors are averaged by using a Gaussian kernel, and the direction to the global maximum of the resulting signal pattern is taken as the gradient direction estimate. The standard deviation of the averaging Gaussian was set to 5% of the spatial extent of the gradient sensor, because this value optimizes the performance of this strategy (5). In ref. 5, time averaging is explicitly implemented by assuming that receptor-generated signals decay with a characteristic time scale. However, we do not include this detail here because for a time-independent gradient, this can be shown to be equivalent to increasing the effective number of receptors by a factor related to the averaging time. Again the performance is reduced compared with the optimal strategy.

Interestingly, although these other strategies do not perform as well as the Bayesian strategy, they nonetheless show the same variation of performance with gradient parameters as the Bayesian strategy. Our experiments therefore do not definitively rule in favor of the optimal strategy compared with one of the others discussed above. To do this would require matching absolute levels of performance, which is currently impossible given our lack of knowledge of the parameters involved in converting a decision regarding gradient direction to directed movement. Nonetheless, this does not undermine the usefulness of our closed-form prediction for relative levels of performance as gradient parameters are varied, and it is still remarkable that our data are consistent with the optimal gradient-sensing strategy.

We now consider an intuitively appealing model for predicting gradient detection performance that gives a substantially worse fit to our data than the curves considered above. We imagine dividing the gradient sensor into 2 compartments separated by a distance d, with $N/2$ receptors in each. In the presence of a gradient, we would expect to observe more bound receptors in one compartment than the other. Taking as a decision criterion the difference in the number of bound receptors between the 2 compartments, we can calculate the expected performance of this model. In a gradient of relative steepness μ and average (dimensionless) background concentration γ, we would expect the difference in the number of bound receptors between to the 2 compartments to be

$$\delta n_{bound} = \frac{N}{2}\left(\frac{\gamma(1+\mu d/2)}{1+\gamma(1+\mu d/2)} - \frac{\gamma(1-\mu d/2)}{1+\gamma(1-\mu d/2)}\right) \approx \frac{N}{2}\mu d \frac{\gamma}{(1+\gamma)^2}$$

and (because the expected number of bound receptors is given by a binomial distribution with event probability $\gamma/(1+\gamma)$) we expect the variance in this difference to be

$$\sigma^2 \approx 2 * \frac{N}{2}\frac{\gamma}{(1+\gamma)^2}.$$

Applying the central limit theorem, for shallow gradients, we would expect the number of correct decisions to be approximately

$$P_{correct} \approx \frac{1}{2} + d\sqrt{\frac{N}{8\pi}}\mu\frac{\sqrt{\gamma}}{1+\gamma}.$$

In contrast to the performance predicted for the optimal strategy, this estimate is symmetric in $\log\gamma$, as seen in Fig. S6. It is also important to understand that, as with the other strategies, we cannot know the absolute scale on the y axis. Thus, in Fig. S6, we have simply shown the functional form of this alternative strategy, matched in maximum performance to the Bayesian strategy. Notable features of this curve are that it achieves its maximum when background concentration is K_d, in contrast to the other curves which

peak at $K_d/2$, and that it decays more slowly at high concentrations. Attempting to fit this function to our experimental data in the same manner as shown in Fig. 3 of the main text both reduces the correlation coefficient and gives a best-fitting K_d value of $\approx$0.1 nM (which agrees less well with the independently determined value of 0.9 nM (4) than the value of 0.3 nM obtained by fitting the optimal strategy).

Statistics

Table S1 shows *N* values for the guidance ratio results reported in Fig. 2*B* of the main paper, and *P* values compared with the plateau condition. Of the 38 samples, 2 failed the Jarque–Bera normality test, therefore for consistency, we used the (nonparametric) Mann–Whitney *U* test for all of the comparisons in this table. *N* values tend to be lower for very high and very low NGF concentrations because a larger proportion of these explants had very low outgrowth, and all explants with outgrowth <1 were rejected from the analysis.

Table S2 shows *P* values comparing the guidance ratios at the peaks of the curves for the different gradient steepnesses (Mann–Whitney *U* test). A Kruskal–Wallis test gave a probability of 0.09 for the null hypothesis that the GR samples corresponding to the peaks in Fig. 2*B* in the main paper come from the same distribution.

Table S3 shows *N* values for the delayed application results (Fig. 3 of main paper), and *P* values comparing the guidance ratio with the plateau condition. In this case, all samples passed the Jarque–Bera normality test, and therefore a 2-sample 2-tailed *t* test was used.

1. Conti AM, Fischer SJ, Windebank AJ (1997) Inhibition of axonal growth from sensory neurons by excess nerve growth factor. *Ann Neurol* 42:838–846.
2. Rosoff WJ, et al. (2004) A new chemotaxis assay shows the extreme sensitivity of axons to molecular gradients. *Nat Neurosci* 7:678–682.
3. Rosoff WJ, McAllister RG, Esrick MA, Goodhill GJ, Urbach JS (2005) Generating controlled molecular gradients in 3D gels. *Biotechnol Bioeng* 91:754–759.
4. Wehrman T, et al. (2007) Structural and mechanistic insights into nerve growth factor interactions with the TrkA and p75 receptors. *Neuron* 53:25–38.
5. Xu J, Rosoff W, Urbach J, Goodhill G (2005) Adaptation is not required to explain the long-term response of axons to molecular gradients. *Development* 132:4545.

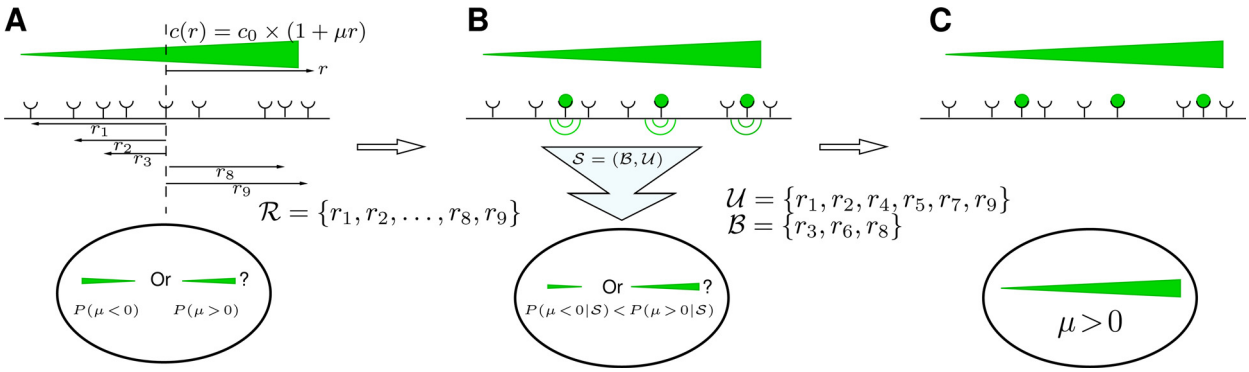

Fig. S1. Bayesian model of spatial gradient detection. (*A*) The model gradient sensor: Receptors located at positions given by the set of displacements $\mathcal{R}$ (for clarity only 9 are shown). The concentration gradient is described by $c(r) = c_0 \times (1 + \mu r)$, where c_0 is the concentration at the center of the gradient sensor, and μ is the relative change in concentration across the sensor's width. (*B*) Signals from the bound and unbound receptors, represented by $\mathcal{S} = (\mathcal{B}, \mathcal{U})$ are interpreted by the intracellular signaling network to assign a relative probability that the gradient points to one side or the other, illustrated by the relative sizes of the gradients schematized in the bubble. (*C*) Finally, the direction is chosen which has the greatest probability of matching that of the gradient.

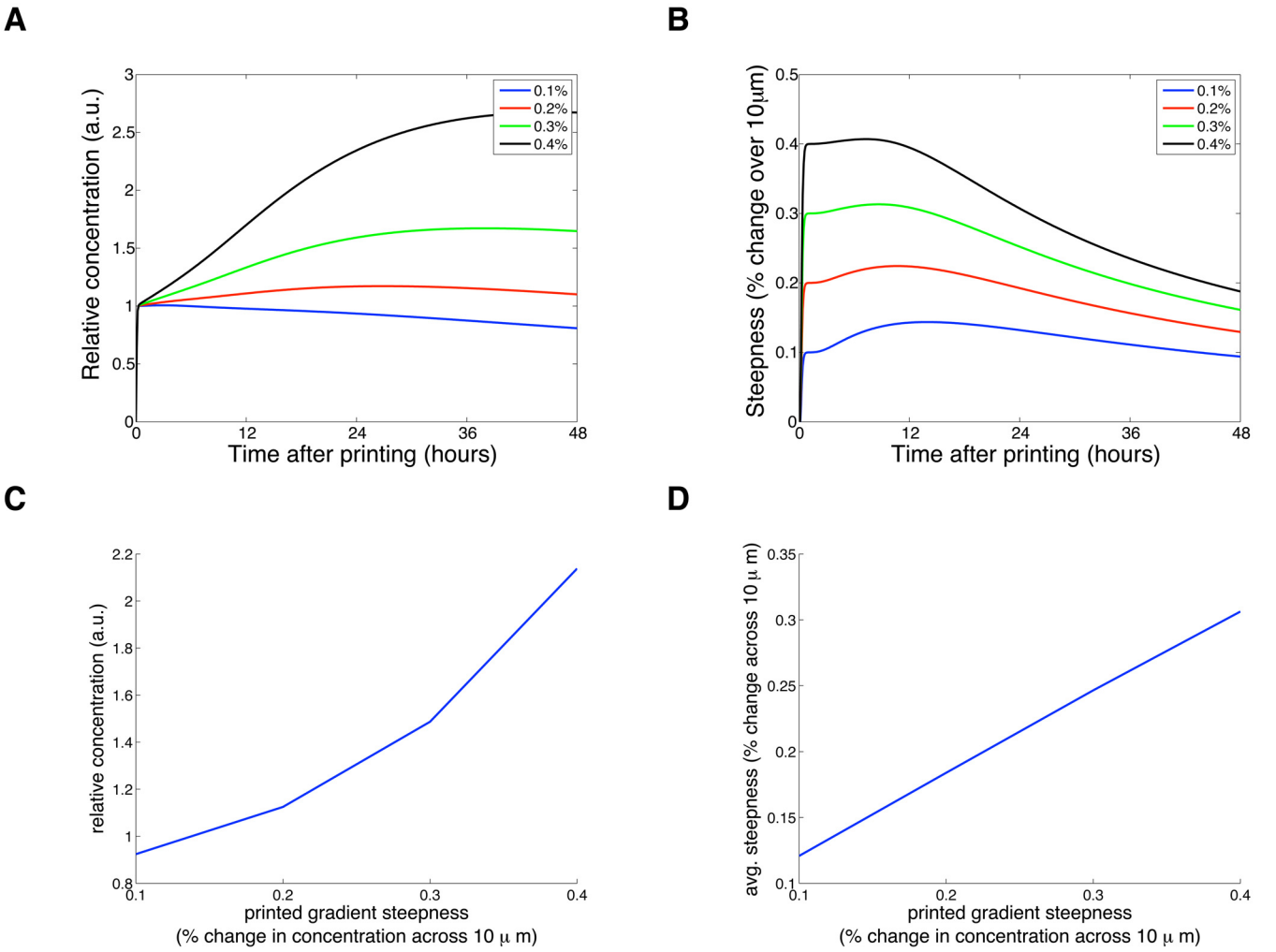

Fig. S2. (*A*) Simulated concentration (arbitrary units) at the explants as a function of time for the different gradients used. (*B*) Simulated gradient steepness as a function of time. (*C*) Calculated concentration correction factors as a function of gradient steepness. (*D*) Calculated gradient steepness correction factors as a function of initial gradient steepness.

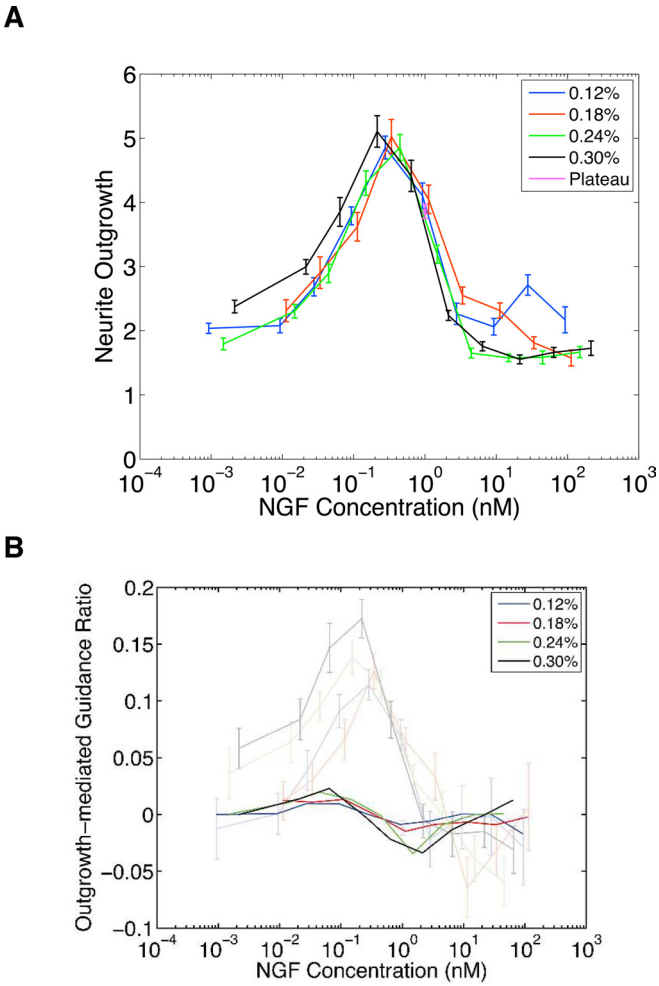

Fig. S3. (*A*) Total neurite outgrowth from explants as a function of absolute concentration and gradient steepness. Note that total outgrowth depends only on absolute concentration and not on gradient steepness. Error bars are SEMs. (*B*) Estimated outgrowth-mediated guidance, with the measured guidance from Fig. 2*B* shown in gray for comparison.

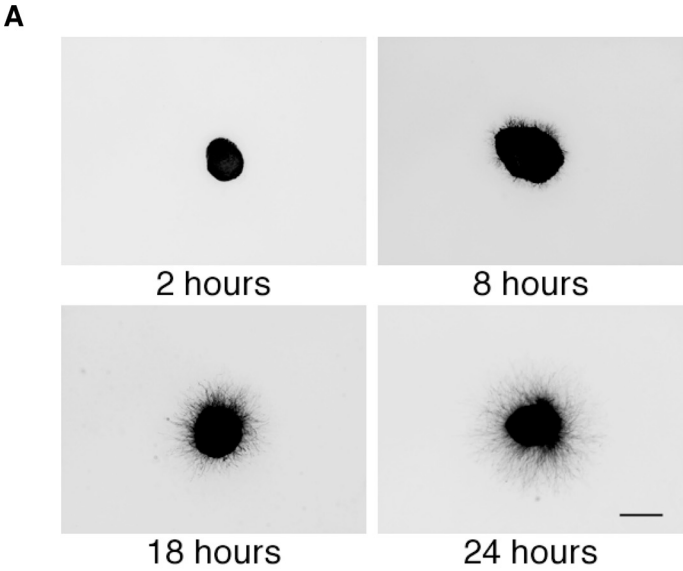

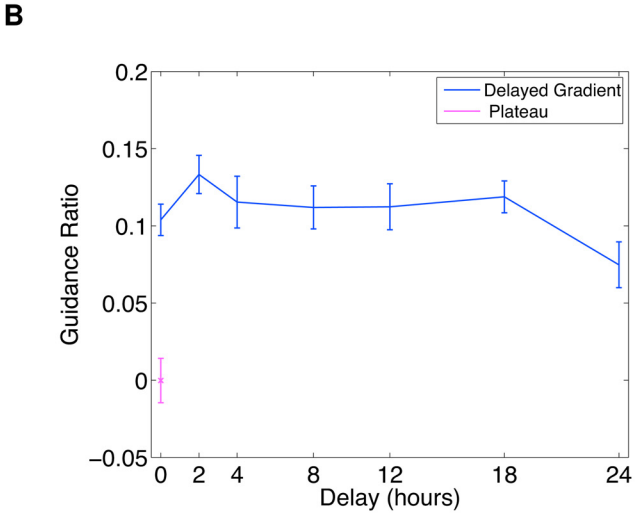

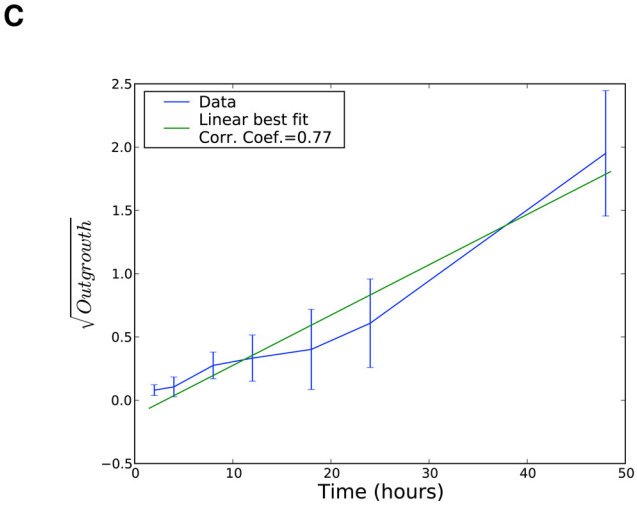

Fig. S4. (*A*) Representative explants showing the degree of growth before gradient application at each of the time points in *B*. (Scale bar, 500 μm.) (*B*) Guidance ratio as a function of the delay between embedding the explants and applying a 0.3 nM/0.24% gradient (*n* and *P* values given in Table S3). Error bars percentages are SEMs. (*C*) Square root of outgrowth plotted against time for DRG explants grown in a 0.1 nM NGF background. The line of best fit is shown in green.

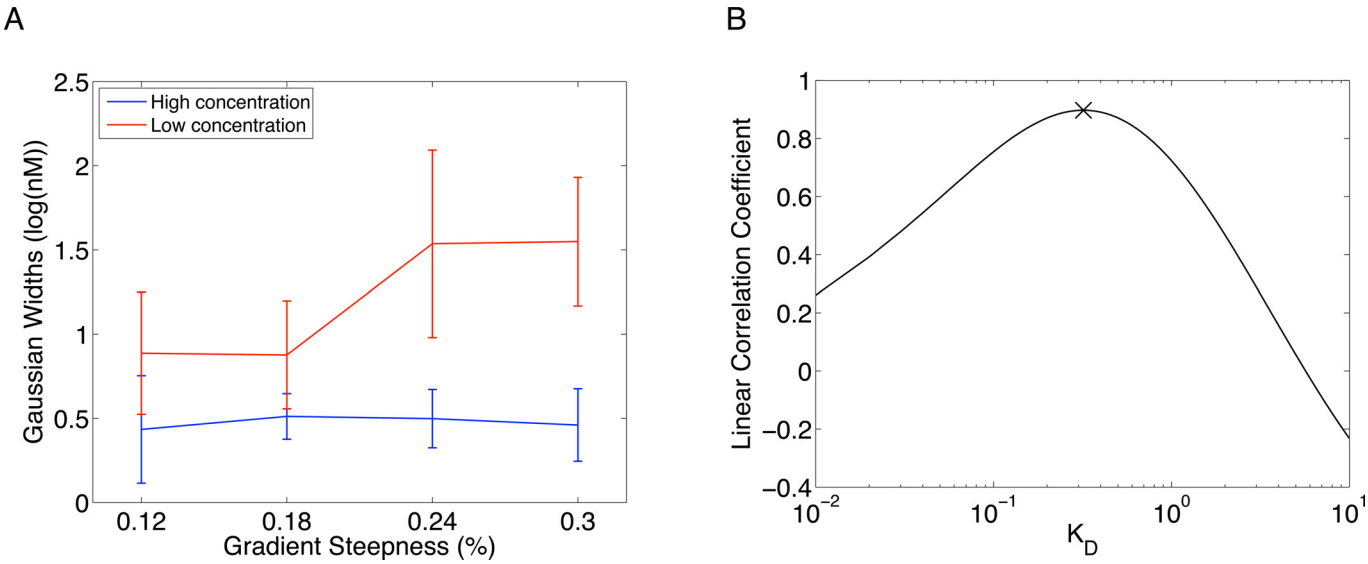

Fig. S5. (*A*) A half-Gaussian function was separately fitted to the low- and high-concentration sides of the GR peak for each gradient steepness. The standard deviation of the fitting Gaussian was consistently larger for the low-concentration side. Error bars represent a numerical estimate of the standard deviation in each of the fitted curve half-widths due to the uncertainty in each of the mean guidance ratios. (*B*) The correlation coefficient between our calculated SNR and measured GR values is maximized for $K_d = 0.3$ nM, taking the value 0.9 at this point (marked by the cross, and quoted in the main text). It can be seen that the model strongly predicts a K_d in the range ≈0.1–1 nM, in agreement with a recent valuederived by Scatchard analysis (3).

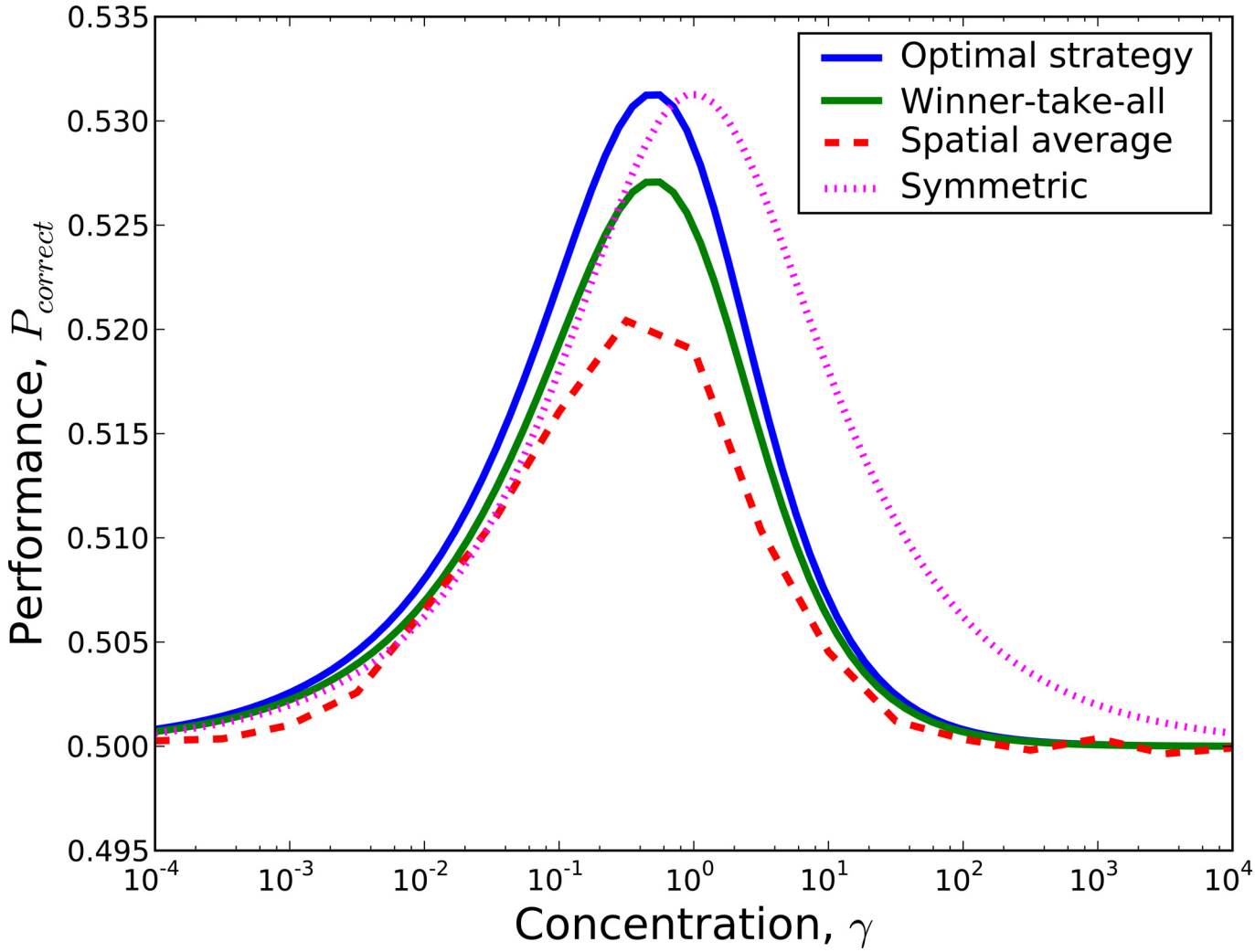

Fig. S6. Performance of alternate gradient sensing strategies. The performance of the optimal strategy is compared with the performance of 3 alternate strategies. The ''winner-take-all'' is an approximation to the Bayesian strategy that estimates the gradient direction by comparing the total number of bound receptors on each side of the gradient sensor. In contrast, the ''spatial averaging'' strategy selects a direction by treating each bound receptor as a spatially displaced δ function, then convolving with a Gaussian filter and selecting the side on which the maximum resulting signal occurs. The ''symmetric'' curve is obtained by considering 2 compartments separated by a distance d with $N/2$ receptors in each compartment. Due to differing assumptions, the absolute performance of this strategy cannot be directly compared with that of the other strategies shown; we have matched the maximum performance of this curve to that of the optimal strategy to make the difference in shape clearer.

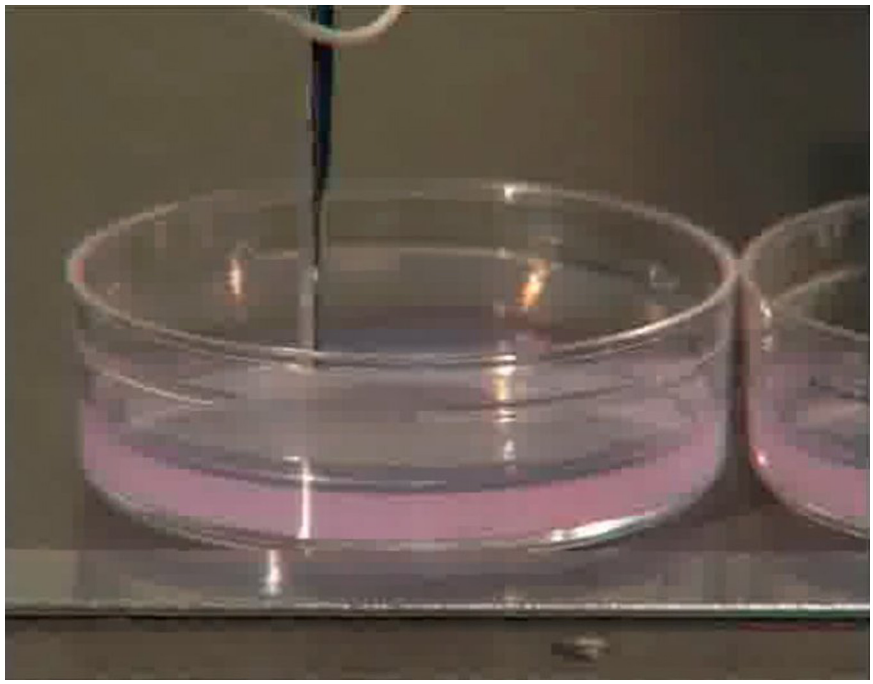

Movie S1. The gradient-printing device. Movie S1 shows the real-time operation of the gradient printing device used for this study (Nanoplotter 2; Gesim). A piezoelectrically operated minipump is used to place precisely controlled volumes of NGF at precisely controlled locations in 35-mm tissue culture dishes. While similar principles were implemented by the device used in ref. 2, the Nanoplotter is much more flexible, reliable, and precise and is easier to control. The operation of the device is entirely computer controlled, and its movements are programmed by using a customized coding language. The programs we used are available on request, as is a higher-resolution version of the movie 927 Mb). First the pump is flushed with water and the tip dried. It then draws a controlled volume of the first NGF stock solution from 1 well if a 96-well plate. The tip is again dried and then travels to a camera/strobe. Test drops are ejected and imaged on the computer screen to verify that the pump is not blocked and that drop size and trajectory are within tolerable limits. The pump then moves to the first 35-mm dish and starts printing onto the surface of the collagen (individual drops are not visible, and the dishes used for this movie contained no explants). No contact is made with the collagen. After printing a line of drops in 1 dish, the pump moves to print the same line in 2 other dishes before collecting the next stock solution of NGF. This reduces both waste of NGF and the total time needed to print multiple dishes. The progress of printing is automatically monitored on the computer screen. When printing with a particular NGF stock is finished, the pump is flushed, and the cycle starts again for printing the next line with a new NGF stock. The movie then cuts to showing the pump printing onto water-sensitive paper, so that the location of the spots can be directly visualized for demonstration purposes. This is the same pattern that is printed on the 35-mm dishes. Each individual spot is made up of 50 individual drops (released at high frequency).

Movie S1 (AVI)

Table S1. Guidance ratio

Gradient, %	[NGF], nM	*N*	*P*	GR
0.12				
	0.00092	29	0.9	−0.01
	0.0092	63	0.6	0.00
	0.028	66	0.006	0.04
	0.092	80	10^{-08}	0.09
	0.28	88	10^{-14}	0.11
	0.92	108	10^{-07}	0.07
	2.8	46	0.8	−0.02
	9.2	38	0.8	−0.00
	28	14	0.9	0.00
	92	15	0.6	−0.03
0.18				
	0.011	64	0.3	0.01
	0.034	71	0.03	0.03
	0.11	75	10^{-05}	0.07
	0.34	74	10^{-14}	0.13
	1.1	113	10^{-06}	0.06
	3.4	49	0.02	0.03
	11	45	0.03	−0.06
	34	50	0.3	−0.03
	110	19	0.6	0.01
0.24				
	0.0015	47	0.1	0.04
	0.015	71	0.0001	0.06
	0.045	90	10^{-10}	0.10
	0.15	91	10^{-16}	0.14
	0.45	94	10^{-15}	0.11
	1.5	112	0.01	0.03
	4.5	74	0.6	0.00
	15	63	0.06	−0.04
	45	36	0.06	−0.06
0.30				
	0.0021	54	0.0006	0.06
	0.021	67	10^{-05}	0.08
	0.064	69	10^{-13}	0.15
	0.21	68	10^{-18}	0.17
	0.64	72	10^{-06}	0.08
	2.1	105	0.8	−0.01
	6.4	82	0.9	−0.02
	21	92	0.6	−0.02
	64	68	0.2	−0.03

The *P* values compare each sample with the plateau condition sample (Mann–Whitney *U* test). For the plateau condition, $N = 438$. GR, guidance ratio.

Table S2. Comparison of guidance ration peaks

	0.18%	0.24%	0.3%	Plateau
0.12%	0.5	0.3	0.008	10^{-14}
0.18%		0.8	0.09	10^{-14}
0.24%			0.02	10^{-16}
0.3%				10^{-18}

P values for the null hypothesis that each pair of peak guidance samples was drawn from the same distribution. Comparisons are also made with the plateau condition (Mann–Whitney *U* test).

Table S3. Delayed application

Delay, h	*N*	*P*	GR
0	124	10^{-08}	0.10
2	85	10^{-10}	0.13
4	59	10^{-06}	0.12
8	60	10^{-07}	0.11
12	59	10^{-07}	0.11
18	96	10^{-10}	0.12
24	88	10^{-03}	0.08
Plateau	59		0.00

Sample sizes and guidance ratios for each condition in the delayed-application experiment are shown with *P* values compared with the plateau condition (2-sample 2-tailed *t* test).